Experimental evaluation of the resolution improvement provided by a silicon PET probe

Brzezinski, K.; Oliver, J. F.; Gillam, J.; Rafecas, M.; Studen, A.; Grkovski, M.; Kagan, H.; Smith, S.; Llosa, G.; Lacasta, C.

Published in:
Journal of Instrumentation

DOI:
10.1088/1748-0221/11/09/P09016

Publication date:
2016

Experimental evaluation of the resolution improvement provided by a silicon PET probe

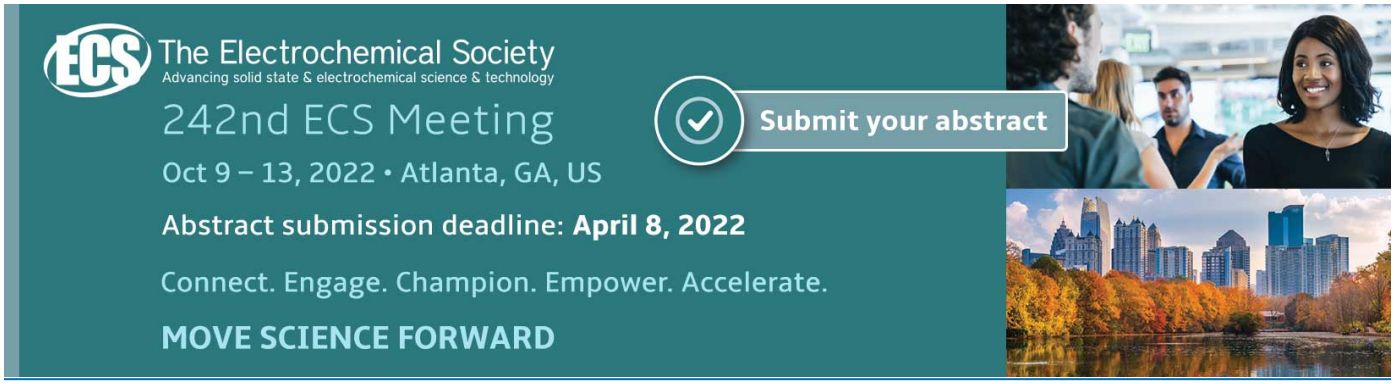

Jinst

Published by IOP Publishing for Sissa Medialab

Received: *July 12, 2016*
Revised: *August 24, 2016*
Accepted: *September 7, 2016*
Published: *September 30, 2016*

Experimental evaluation of the resolution improvement provided by a silicon PET probe

K. Brzeziński,[a,b,1] **J.F. Oliver,**[a] **J. Gillam,**[a,c] **M. Rafecas,**[a,d] **A. Studen,**[e] **M. Grkovski,**[e,f] **H. Kagan,**[g] **S. Smith,**[g] **G. Llosá,**[a] **C. Lacasta**[a] **and N.H. Clinthorne**[h]

[a] *Instituto de Física Corpuscular, CSIC/Universitat de València, C/ Catedrático José Beltrán 2, Paterna, Valencia, Spain*
[b] *KVI-Center for Advanced Radiation Technology, University of Groningen, Zernikelaan 25, Groningen, The Netherlands*
[c] *Faculty of Health Sciences, University of Sydney, 94 Mallett St., Camperdown, NSW, Australia*
[d] *Institute of Medical Engineering, University of Lubeck, Ratzeburger Allee 160, Lübeck, Germany*
[e] *Jožef Stefan Institute, Jamova cesta 39, Ljubljana, Slovenia*
[f] *Department of Medical Physics, Memorial Sloan Kettering Cancer Center, 1275 York Avenue, New York, NY, U.S.A.*
[g] *Department of Physics, Ohio State University, 191 West Woodruff Ave, Columbus, OH, U.S.A.*
[h] *Department of Radiology, University of Michigan, 1500 E. Medical Center Drive, Ann Arbor, MI, U.S.A.*

E-mail: k.w.brzezinski@rug.nl

Abstract: A high-resolution PET system, which incorporates a silicon detector probe into a conventional PET scanner, has been proposed to obtain increased image quality in a limited region of interest. Detailed simulation studies have previously shown that the additional probe information improves the spatial resolution of the reconstructed image and increases lesion detectability, with no cost to other image quality measures. The current study expands on the previous work by using a laboratory prototype of the silicon PET-probe system to examine the resolution improvement in an experimental setting. Two different versions of the probe prototype were assessed, both consisting of a back-to-back pair of 1-mm thick silicon pad detectors, one arranged in 32 × 16 arrays of 1.4 mm × 1.4 mm pixels and the other in 40 × 26 arrays of 1.0 mm × 1.0 mm pixels. Each detector was read out by a set of VATAGP7 ASICs and a custom-designed data acquisition board which allowed trigger and data interfacing with the PET scanner, itself consisting of BGO block detectors

[1] Corresponding author.

doi:10.1088/1748-0221/11/09/P09016

2016 JINST 11 P09016

segmented into 8 × 6 arrays of 6 mm × 12 mm × 30 mm crystals. Limited-angle probe data was acquired from a group of Na-22 point-like sources in order to observe the maximum resolution achievable using the probe system. Data from a Derenzo-like resolution phantom was acquired, then scaled to obtain similar statistical quality as that of previous simulation studies. In this case, images were reconstructed using measurements of the PET ring alone and with the inclusion of the probe data. Images of the Na-22 source demonstrated a resolution of 1.5 mm FWHM in the probe data, the PET ring resolution being approximately 6 mm. Profiles taken through the image of the Derenzo-like phantom showed a clear increase in spatial resolution. Improvements in peak-to-valley ratios of 50% and 38%, in the 4.8 mm and 4.0 mm phantom features respectively, were observed, while previously unresolvable 3.2 mm features were brought to light by the addition of the probe. These results support the possibility of improving the image resolution of a clinical PET scanner using the silicon PET-probe.

KEYWORDS: Gamma camera, SPECT, PET PET/CT, coronary CT angiography (CTA); Medical-image reconstruction methods and algorithms, computer-aided software

2016 JINST 11 P09016

Contents

2016 JINST 11 P09016

1 Introduction

There is a sustained effort in positron emission tomography (PET) research to improve the spatial resolution achievable in clinical scanners. In modern PET/CT (computerized tomography) devices, the reconstructed PET resolution is typically 4–6 mm [1], relatively low compared to the sub-millimeter resolution available in the CT image. PET resolution is limited mainly by the size of the detector elements, as well as the effects of positron range and photon acollinearity [2]. However, the reduction of the physical size of the detector elements may lead to lower sensitivity, through losses caused by Compton scattering and a reduction of packing fraction [3].

The PET-insert concept, involving the introduction of high-resolution detectors into the field of view (FOV) of a conventional scanner, has been studied as a method of increasing the spatial resolution of PET images over a localized region of interest. Several groups have explored such an approach using both ring-insert geometries [4–6], where the high-resolution detectors form a ring (or partial ring) within the conventional PET ring, and probe geometries [7, 8], where a single detector module is placed at a specific location. In such geometries, the fine segmentation of the insert detector does not reduce the statistical quality of the data; rather, counts are added as sensitivity is increased by the presence of the extra detector. Furthermore, placing the insert detectors in closer proximity to the annihilation location reduces the effect of acollinearity. Following the probe geometry, we have proposed a high-resolution silicon (Si) PET probe system, which employs a layered Si detector module in the FOV of a clinical whole-body scanner. Our previous simulation

studies [9] considered a probe module containing 10 Si detectors, each an 80 × 52 array of $1 \times 1 \times 1\,mm^3$ pixels and stacked with 1-mm spacing, in coincidence with the Siemens Biograph64 PET scanner. We demonstrated that with the addition of the probe the spatial resolution of the images obtained by the Biograph was increased by factors of up to 2 and lesion detectability improved, without degrading other figures of merit such as contrast or spill-over ratio (SOR). The current work is an experimental demonstration of the Si PET probe system and, therefore, complementary to the investigations performed in our previous simulation studies.

The current study makes use of a laboratory PET-insert prototype, which utilizes high-resolution Si detectors in coincidence with a table-mounted whole-body BGO PET scanner [4]. The setup has been used in previous works for examining several Si PET-insert geometries, focusing on the ring-insert and partial-ring configurations [4, 6]. While Grkovski et al. [6] presented images obtained using the Si detector module at several angular positions (partial ring geometry), the current study examines an arrangement where the module is fixed at one position, thus mimicking the PET probe system presented in our previous simulation studies [9]. Furthermore, choosing a shorter acquisition time than Grkovski et al. [6], in order to obtain data of similar statistical quality as that used in simulation [9], allows for a closer validation of the original simulated system.

2 Methods

2.1 System setups

The PET scanner used in this study consisted of two partial rings using 24 block detectors from a decommissioned CTI 931 PET scanner. The blocks were organized into two groups of 12, directly opposite one another at a radius of 500 mm, with each spanning 67.5 degrees (out of 180). To emulate the complete ring, the object being imaged was set on a rotating stage at the centre of the FOV and rotated to several positions during data collection. Each block detector consisted of 32 BGO crystals, each with dimensions 6 mm × 12 mm × 30 mm thick, in an 8 × 4 array (8 circumferential and 4 axial). Each BGO block was coupled to a 2 × 2 array of photomultiplier tubes (PMTs) and interaction positions estimated by light-sharing [4]. Further details on the PET scanner can be found in Clinthorne et al. [4]. The external PET ring was used for all geometries studied. The setup is shown in figure 1.

Two types of 1-mm-thick Si pad detectors were used for the experimental systems, according to their availability during the experimental schedule. The difference between the two sensors is not significant for the conclusions of the study. The first consisted of 32 × 16 arrays (512 total) of 1.4 mm × 1.4 mm pads, the second of 40 × 26 arrays (1040 total) of 1.0 mm × 1.0 mm pads. Both types were organized into modules made up of two face-to-face detectors, separated by a 0.8 mm gap. Each detector was read out by a set of VATAGP7 ASICs and a custom-designed data acquisition board, which allowed trigger and data interfacing with the PET scanner. Further details on the Si detector modules can be found in Grkovski et al. [6] (1040-pad detectors) and Clinthorne et al. [4] (512-pad detectors). The modules were placed in light-tight housing and mounted on opposing sides of the rotating stage, as shown in figure 1. This geometry serves the dual purpose of both probe and ring-insert experiments. In the present work, only the probe-based aspects of the device are explored.

2016 JINST 11 P09016

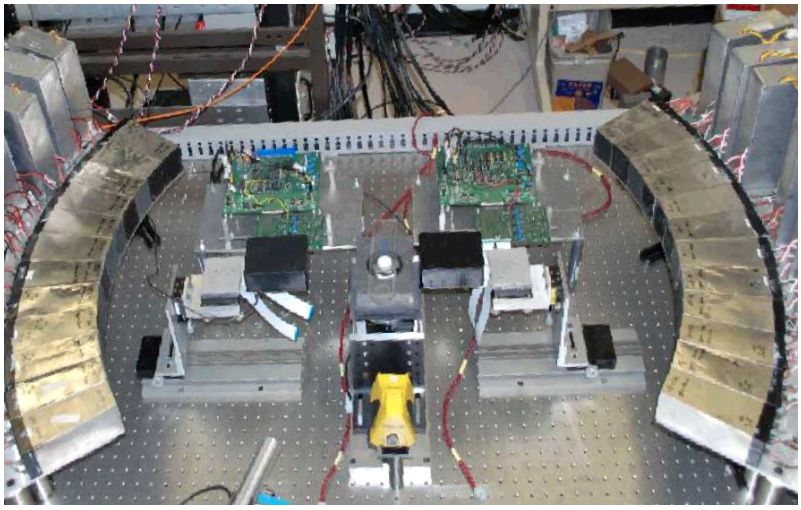

Figure 1. Photograph of the experimental setup. Visible in the centre is lead shielding surrounding the phantom, with two black boxes on either side housing the Si detectors, and, further away, the two partial-rings of BGO block detectors.

For each detector in the setup, trigger and position information was routed to a data acquisition system that included a field programmable gate array (FPGA) that combined trigger signals to form coincidence events, which were stored as a list, available for post-processing and image reconstruction. A detailed description of the data acquisition system and coincidence logic may be found in Grkovski et al. [6].

Four types of coincidence events may be formed using such a setup: BGO-BGO events, where each photon is detected in opposing BGO groups; two types of Si-BGO events, where one photon is detected in one or the other BGO group and the other in its opposing Si detector; and Si-Si events, where each photon is detected in opposing Si detectors. Si-Si events are only available in the ring-insert geometry and are not considered in this study. BGO-BGO events simulate the regular PET ring data when the phantom is rotated through 360°. Si-BGO events with the Si module at a single location comprise what will be referred to as "probe" data.

2.1.1 Two-dimensional setup

A two-dimensional geometry was set up using the 1040-pad Si detector modules. These were placed on opposite sides of the centre of the FOV, with the long edge of the detectors facing the centrally located phantom, offset by 108 mm. Lead shielding was placed around the phantom, leaving only a 1 mm slit through which annihilation photons could escape. The collimation was aligned with the edge of one detector from each Si pair and resulted in only one axial row of BGO crystals being involved in detection. A schematic diagram illustrating the collimated setup is shown in figure 2. The lead shielding around the phantom can be seen in figure 1. In order to demonstrate the probe principle using this setup, data from two specific rotational positions of the phantom were used, each separated by 180°, which were isolated from full-rotation Si-BGO data. At each of the two positions, data from one or the other Si module was isolated, resulting in two Si-BGO datasets that contain the same projection angles. Fully tomographic BGO-BGO data was obtained by rotating the phantom through the 360° in 6° steps, with the Si modules in place.

2016 JINST 11 P09016

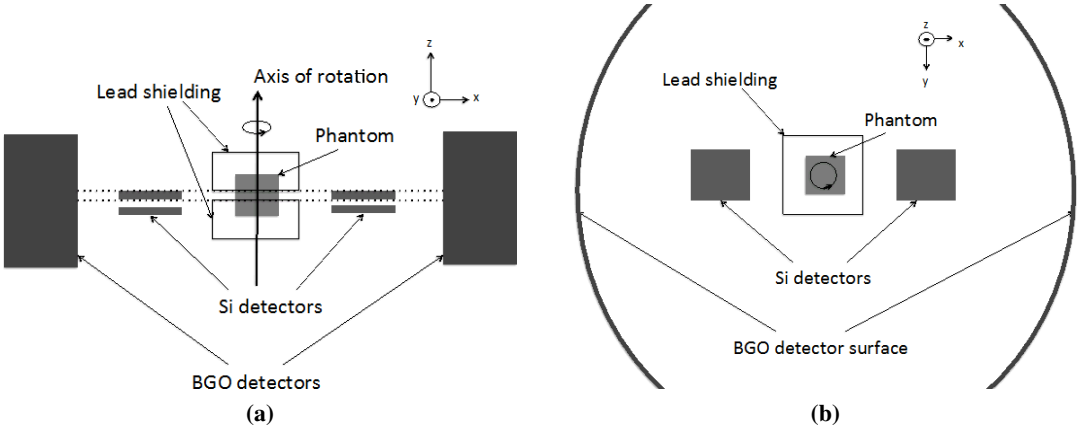

Figure 2. Diagram of the 2D geometry showing a) the side view and b) the top view. The drawing is not to scale. The centres of the Si detectors are both 108 mm away from the centre of the FOV. The phantom rotating through 360 degrees simulates a Si ring while a stationary phantom corresponds to two probe positions.

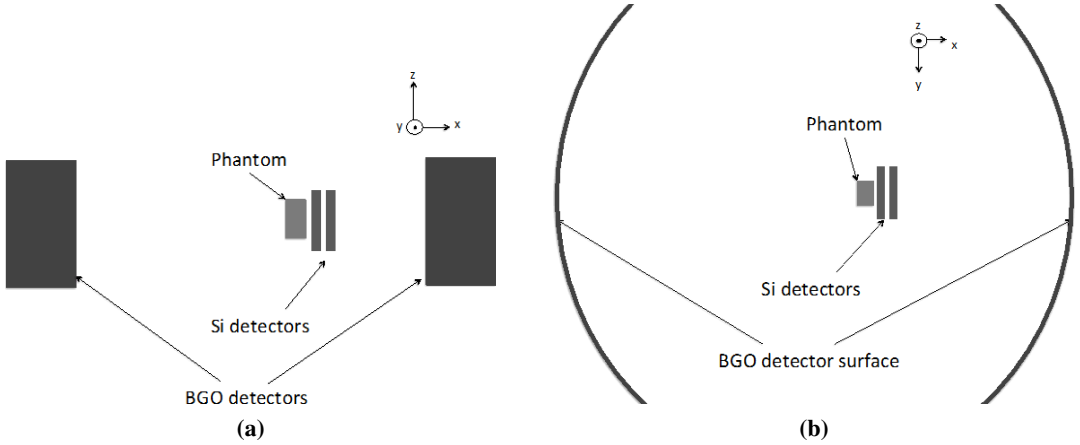

Figure 3. Diagram of the 3D probe geometry showing a) the side view and b) the top view. The phantom is placed in close proximity to the probe. The drawing is not to scale.

2.1.2 Three-dimensional setup

For the three-dimensional geometry, the 512-pad Si detectors were used. To achieve fully 3D images, the collimation was removed and one Si detector module placed face-on to the object being imaged (as opposed to edge-on) at an offset of 97 mm from the centre of the FOV. In this configuration, both detectors in the module face the phantom and all axial BGO detector rows participate in measurement. A schematic diagram illustrating the 3D setup is shown in figure 3, with the phantom in close proximity to the probe. To obtain probe data the phantom was not rotated, collecting Si-BGO events for a single angular position.

2.2 Image reconstruction

Data were reconstructed using a modified version of the list-mode ML-EM algorithm described in our previous work [9]. The system matrix elements were calculated on-the-fly using a multi-line Siddon method. The end-points of the Siddon lines were randomly distributed throughout the BGO

2016 JINST 11 P09016

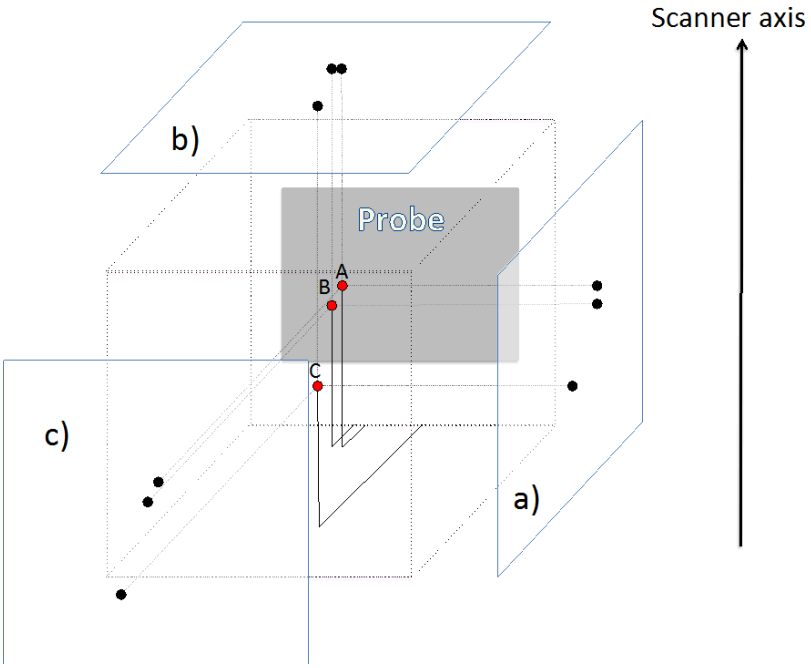

Figure 4. Schematic diagram of the positions and orientation on the three ^{22}Na point-like sources relative to the probe location and imaging planes. The sources and imaging planes are identified with letters for reference.

crystal and randomly at the half-depth plane for the Si pixels, using three and two-dimensional uniform distributions respectively. This step was performed on the list-mode coincidence file prior to reconstruction. Attenuation in the BGO was not accounted for in lines originating from a finite depth within the detector crystal. A fine image grid of $0.2 \times 0.2 \times 0.2\,\text{mm}^3$ voxels was used for the reconstructions. For both the 2D and the 3D geometries, 100 Siddon lines per measurement were implemented and used. Corrections for sensitivity, random coincidences, scatter and attenuation, both in detectors and other hardware, were not implemented. All images were convolved with a Gaussian function of 0.4 mm FWHM in post-processing.

2.3 Resolution of the probe data

3D probe data was acquired using a group of three low-activity sodium-22 (^{22}Na) point-like sources and no phantom rotation. The phantom was placed as close as possible to the probe by attaching it directly to the probe's plastic casing, about 1.5 and 2.3 cm away from each of the two Si detectors respectively. BGO-BGO data was not collected in this setup. Figure 4 shows a schematic diagram of the orientation of the point-like sources relative to the probe. Expected projections onto three orthogonal planes are also shown in the figure for reference during analysis. The sources were oriented so that the 1.5 mm segment between points A and B (in figure 4) was aligned parallel to the surface of the Si detectors.

2.4 Imaging study

Data was obtained for a Derenzo-like hot-spot resolution phantom, filled with low-activity ^{18}F-FDG solution, using the 2D detector setup. A diagram indicating the sizes of the phantom inserts is

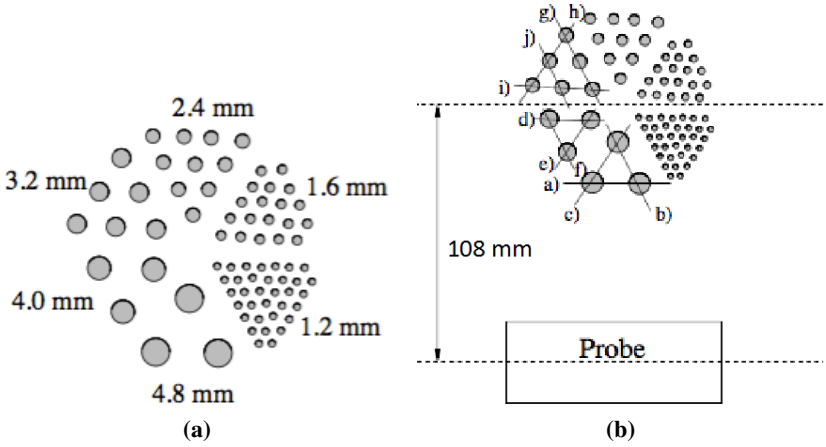

Figure 5. Diagram of the Derenzo-like phantom showing: a) the sizes of the insert rods and b) the orientation relative to the Si detectors used in the study. Probe size and distance to the phantom are not to scale in b), while profile locations are shown for reference.

shown in figure 5a. For the probe data, events were extracted from the full Si-BGO dataset by limiting phantom angular position to the two rotations where the 4.8-mm phantom features were at their closest to a Si module, matching the arrangement sketched in figure 5b, where "Probe" is equivalent to the detector position of a particular Si module. This occurred at two rotational positions, separated by 180 degrees, once for each Si module. At each instance, 0.67×10^5 and 0.68×10^5 events were collected and combined to give a total Si-BGO dataset sample of 1.35×10^5 events. In a separate acquisition, 9.31×10^5 full-rotation BGO-BGO events were obtained and reconstructed to form the PET ring image. To create the probe-enhanced image, 1.35×10^5 randomly selected BGO-BGO events were replaced with the same number of probe events, and the combination reconstructed. The probe data thus made up 15% of the combined total of 9.31×10^5. In this way, the comparison could be made between probe-enhanced and PET ring-only images of similar statistical quality.

Line profiles were taken through the sections of the phantom where individual features were distinguishable in the ring-only image. These include the sections with the three largest features, of diameter 4.8 mm, 4.0 mm and 3.2 mm. Figure 5b shows a diagram of the phantom with the labeled profile locations. Also included in the figure is the relative position of the probe, which is not shown to scale. Peak-to-valley ratios were calculated from several line profiles.

3 Results

3.1 Resolution of the probe data

Figure 6 shows images reconstructed from the 3D probe data acquired using the ^{22}Na point-source phantom. The three images were obtained by summing all volume slices in three orthogonal directions, corresponding to the three planes shown in figure 4. Points A and B are clearly differentiated in figure 6a, which shows the summed transaxial slices, and c), representing the axial slices which are parallel to the probe surface. The images demonstrate a spatial resolution

2016 JINST 11 P09016

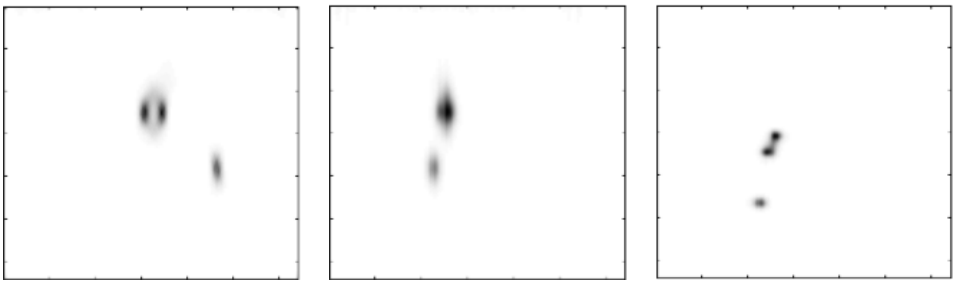

(a) (b) (c)

Figure 6. Images reconstructed from Si-BGO data in the 3D probe configuration. Summed slices of three orthogonal planes are shown: a) the transaxial, b) and c) two axial planes. The summed slices in c) are what is seen from the probe's point of view. The images correspond to the projections described in figure 5b. The color scale is inverted for better visualization.

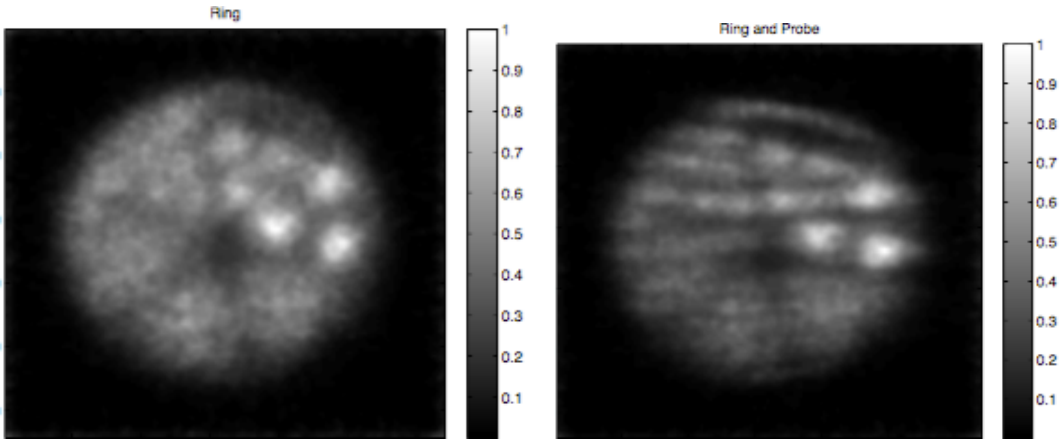

(a) (b)

Figure 7. Images of the resolution phantom from the 2D probe setup. Shown are images reconstructed using a) ring (BGO-BGO) data only and b) including probe data. The Si detector is to the right of the image.

of less than 1.5 mm FWHM at this position, about 1 cm away from the probe's surface. This is a significant improvement from the 6 mm resolution of the BGO scanner [4]. The two points are indistinguishable in figure 6b since they lay in different slices one behind the other and overlap when the slices are summed.

3.2 Imaging study

Images of the Derenzo-like phantom are displayed in figure 7, with a) showing the ring-only image, reconstructed from BGO-BGO events only, and b) the image that also includes the probe data. An improvement in resolution is clearly visible, especially in the 3.2 mm features. The directionality of this improvement, with largest resolution increase occurring in the direction parallel to the surface of the probe, can also be seen. This is in agreement with simulation studies [8, 9].

The improvement can be further observed by looking at the line profiles through the sections of the phantom that are described in figure 5b. These profiles are plotted in figure 8. The profiles that are taken perpendicular to the probe, such as g), j) and f), do not show significant improvement. The

2016 JINST 11 P09016

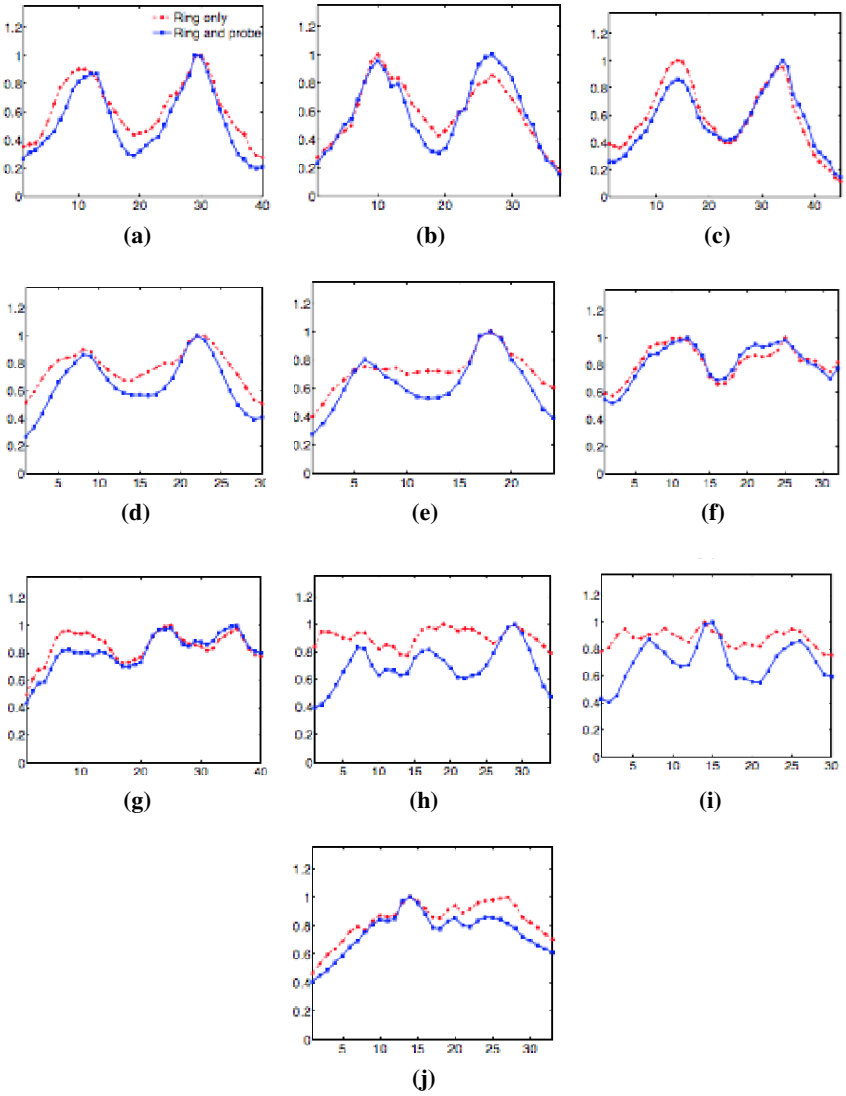

Figure 8. Comparison of profiles through the resolution phantom as defined in figure 5b. Red lines represent the ring-only image and blue the one where probe data is included. The values on the ×-axis are in millimeters and on the y-axis they represent normalized intensity, where a value 1 is maximum.

largest resolution increase is observed in profiles taken in the direction parallel to the probe surface. This improvement is most notable in the region containing the 3.2 mm inserts (profiles h and i). Here, features that were unresolvable in profiles through the ring-only image are revealed through the addition of the probe. In the 4.0-mm section of the phantom, an improvement in peak-to-valley ratio of 38% may be observed with the addition of the probe (profiles d and e). In the region closest to the probe, which contains the 4.8-mm inserts, this improvement reaches 50% (profile b).

4 Discussion

For the present studies, a laboratory Si PET insert prototype was adapted to acquire data for two distinct probe geometries, based on the Si PET probe concept presented in previous simulation studies [9]. The image grid of $0.2 \times 0.2 \times 0.2\,\mathrm{mm}^3$ voxels was used in order to resolve the finest

2016 JINST 11 P09016

phantom features, which were within the expected resolution capabilities of the highest resolution data (Si-Si events) [6]. The resulting increase in image pixel density, by a factor of 125 from the $1 \times 1 \times 1\,\mathrm{mm}^3$ image grid used in previous simulation studies [9], would indicate that an increase in the number of Siddon lines per detector pair is required. Furthermore, larger scintillation crystals in the scanner also motivate such an increase. 100 Siddon lines were used as an initial estimate. However this number may be optimized in future studies for shorter reconstruction times. Corrections for sensitivity, randoms, scatter and attenuation were also left to future work.

The images were convolved with a Gaussian function in order to reduce the undersampling artefacts created by reconstructing the low-resolution data on the fine $0.2 \times 0.2 \times 0.2\,\mathrm{mm}^3$ voxels. This was considered a more efficient approach of overcoming the artefacts than further increasing Siddon-ray count, to which reconstruction time is directly proportional. The value of 0.4 mm FWHM was chosen as adequate in reducing the sampling artefacts, while remaining below the highest resolution achievable in Si-BGO data [4].

During the acquisition of the 3D probe data, the phantom was placed as close as possible to the Si detectors in order to investigate the highest resolution achievable by the probe system. BGO-BGO data could not be collected in this setup, as the off-centre position of the phantom did not allow for its required rotation. The apparent elongation of the point-like sources in the resulting images is due to data truncation. When reconstructing only probe events, very limited projection angles are available. Lines of response (LORs) in the probe data are nearly parallel to each other and approximately perpendicular to the face of the stationary probe. Since resolution improvement is limited to the plane perpendicular to the LORs, data truncation results in excellent resolution in planes parallel to the face of the probe and limited resolution in the direction perpendicular to it. Depending on the slice orientation, features will appear elongated in the prevailing LOR direction (vertical in figures 6a and 6b), or sharp as in figure 6c. Similar behaviour was reproduced in the simulation study [9].

Previous studies have shown that in the area close to the probe the resolution of its own detectors dominates the spatial resolution of the combined probe-and-ring system [9]. The high resolution observed in this study suggests similar performance when the probe data is added to that of the PET ring.

In the imaging study using the Derenzo-like phantom, the number of probe events emitted from a single 1-mm axial slice of the phantom corresponded roughly to that expected given the $5{\times}10^6$ events used in previous simulations [9], which included the entire axial extent of the phantom and scanner. The choice of using 15% probe events was also based on the previous simulation studies [9] using the same phantom. The simulations gathered 30% probe events, but in the experimental study the distance between the phantom and the Si detectors was roughly doubled and, therefore, the angle subtended by the detectors at the centre of the phantom roughly halved. Using this angle as representative of probe sensitivity, half of the simulated quantity of the probe data was considered an appropriate estimate. For the PET ring image, the same total number of BGO-BGO events was used as for the combined probe and ring image, thus eliminating sensitivity as an influencing factor.

From the images of the Derenzo-like phantom, it is notable that the increase in resolution is observed at distances beyond 100 mm from the probe, substantially further than observed using the simulated system in previous studies [9], where the probe provided improved resolution up to a distance of 50 mm away from its surface. This may be due to the lower resolution of the PET ring

2016 JINST 11 P09016

detectors in the experimental setup as compared to those in the simulation study and, as a result, of the PET ring image that is enhanced by the probe data. In the simulation study [9], the Siemens Biograph64 PET scanner already produced images of relatively high resolution on its own, which made it more challenging to enhance.

In the images of the Derenzo-like phantom, the directionality of the resolution enhancement makes the circular cross-section of some of the phantom features appear oblate, giving the impression that they are elongated. This apparent elongation is a result of improved resolution, which is limited to the direction perpendicular to the probe LORs. That is to say, the circular features are shortened in one direction. This effect is made evident by the line profiles.

The increased directional limitation of the resolution enhancement in the present work, compared to the previous simulation studies [9] where this effect was not observed, may be caused by data truncation, which is the result of the larger distance to the probe and the shorter length of the probe detector facing the phantom. These two factors limit the number of projection angles available at the phantom location. Furthermore, the larger size of the BGO crystals in the experimental setup, compared to those of the simulated Biograph ($4 \times 4 \times 20\,\mathrm{mm}^3$), produces a larger difference between probe and PET ring resolutions in the experimental system. This increases the impact of the probe on ring data, which in this case only occurs in one direction. The apparent elongation of phantom features when using the probe may deceive an observer into believing that circular features are oblate. In order to overcome this effect, multiple probe positions may be considered during data acquisition.

5 Conclusions

In the present work, we have extended our previous investigations into a high-resolution PET system that incorporates a silicon (Si) detector probe into a clinical PET scanner. The ability of such a device to improve the spatial resolution of a conventional scanner has been experimentally demonstrated using a laboratory PET setup and two different prototypes of the Si probe. Using a group of three point-like sources at a distance of around 1–2 cm from the probe, a resolution of 1.5 mm FWHM was measured by reconstructing the probe data alone, much higher than the approximately 6 mm FWHM resolution achievable by the PET ring. The high spatial resolution obtained from the probe data is an indication of the potential for similar results in combined probe-and-ring images in areas close to the probe where this high-resolution data is dominant. The experimental setup limited resolution measurements for the combined probe-and-ring system to distances of on the order of 100 mm, where improvement was observed using a Derenzo-like phantom. Features of 3.2 mm in diameter, undetectable to the PET scanner alone, were brought to light using the Si probe. Larger features also showed augmented resolution, with peak-to-valley ratios improving by up to 50%. The techniques described in this work are a promising approach for achieving enhanced resolution in region-of-interest imaging in a conventional PET scanner. Furthermore, the results presented provide further evidence that such techniques can be implemented in an experimental apparatus, thus further motivating their clinical implementation.

2016 JINST 11 P09016

Acknowledgments

This work was partially supported by Spanish Ministry of Science and Innovation, grant FPA2010-14891, and the European Commission under FP7 EURATOM-FISSION Grant 212100 (MADEIRA). Karol Brzezinski was supported by the Consejo Superior de Investigaciones Cientificas (CSIC) through the JAE-Predoc contract.

References

[1] P.B. Zanzonico, *Radionuclide imaging*, in *Essentials of in vivo biomedical imaging*, S.R. Cherry, R.D. Badawi and J. Qi eds., CRC Press, Boca Raton Florida U.S.A. (2015).

[2] W.W. Moses and S.E. Derenzo, *Empirical observation of resolution in positron emission tomographs utilizing block detectors*, *J. Nucl. Med.* **34** (1993) 232.

[3] R. Fontaine, *Design considerations for positron emission tomography (PET) scanners dedicated to small-animal imaging*, in *Electronics for Radiation Detection*, K. Iniewski ed., CRC Press, Boca Raton Florida U.S.A. (2010).

[4] N. Clinthorne et al., *Silicon as an unconventional detector in positron emission tomography*, *Nucl. Instrum. Meth.* **A 699** (2013) 216.

[5] H. Wu, D. Pal, T.Y. Song, J.A. O'Sullivan and Y.C. Tai, *Micro insert: A prototype full-ring PET device for improving the image resolution of a small-animal PET scanner*, *J. Nucl. Med.* **49** (2008) 1653.

[6] M. Grkovski et al., *Evaluation of a high resolution silicon PET insert module*, *Nucl. Instrum. Meth.* **A 788** (2015) 86.

[7] S. Huh, N.H. Clinthorne and W.L. Rogers, *Investigation of an internal PET probe for prostate imaging*, *Nucl. Instrum. Meth.* **A 579** (2007) 339.

[8] J. Zhou and J. Qi, *Theoretical analysis and simulation study of a high-resolution zoom-in PET system*, *Phys. Med. Biol.* **54** (2009) 5193.

[9] K. Brzezinski, J.F. Oliver, J. Gillam and M. Rafecas, *Study of a high-resolution PET system using a silicon detector probe*, *Phys. Med. Biol* **52** (2014) 6117.

2016 JINST 11 P09016